SUPPORTING INFORMATION

Atomic structures and gram scale synthesis of three tetrahedral quantum dots

*Alexander N. Beecher[1#], Xiaohao Yang[2#], Joshua H. Palmer[1], Alexandra L. LaGrassa[1], Pavol Juhas[3], Simon J. L. Billinge[2,3], Jonathan S. Owen[1]**

[1]Department of Chemistry, Columbia University, New York, New York 10027, United States

[2]Department of Applied Physics and Applied Mathematics, Columbia University, New York, New York 10027, United States

[3]Condensed Matter Physics and Materials Science Department, Brookhaven National Laboratory, Upton, New York 11973, United States

[#]These authors contributed equally to this work.

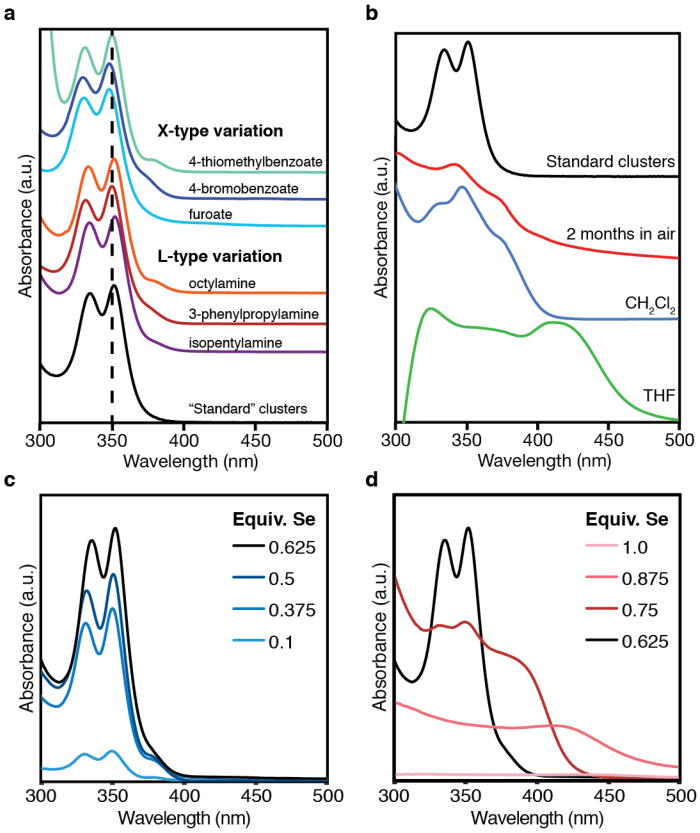

Figure S1. Quantum dot derivatives, stability, and stoichiometry. (**a**) UV-Vis spectra of **CdSe$_{(350\ nm)}$** prepared with various primary amines and carboxylates. Regardless of the change, little effect is observed in the UV-Vis profile suggesting that the structure of the inorganic core is preserved. (**b**) UV-Vis of QDs taken in toluene before and after exposure to air (red, middle top), dichloromethane (blue, middle bottom), or tetrahydrofuran (green, bottom) demonstrating sensitivity of QDs to various conditions. (**c**) The effect of varying Cd:Se stoichiometry on the synthesis of **CdSe$_{(350\ nm)}$**. Increasing amounts of $(TMS)_2Se$ are added to a solution containing one equivalent of cadmium benzoate and two equivalents of *n*-$BuNH_2$. Initially, additional $(TMS)_2Se$ is directly converted into **CdSe$_{(350\ nm)}$** to increase yield, but above 0.625 equivalents (**d**), **CdSe$_{(350\ nm)}$** begins to deteriorate. At a 1:1 ratio of Cd:Se, bulk CdSe precipitates.

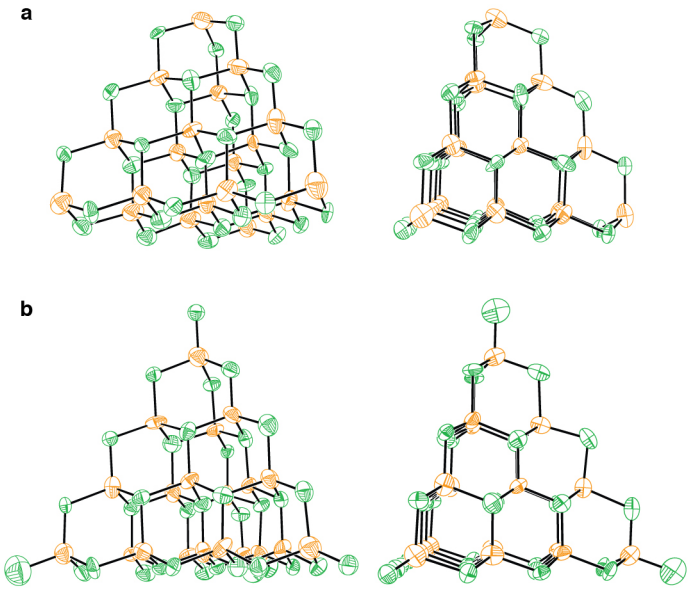

Figure S2. Two views of the $Cd_{31}Se_{20}$ core structure (**a**) and two views of the $Cd_{35}Se_{20}$ core structure (**b**) (Se is orange, Cd is green). Thermal ellipsoids are set at the 30% probability level.

Table S1. **$CdSe_{(350\ nm)}$** single crystal, intensity collection and refinement data.

	$Cd_{31}Se_{20}$	$Cd_{35}Se_{20}$
lattice	Orthorhombic	Orthorhombic
assumed formula	$Cd_{31}Se_{20}C_{242}H_{352}N_{22}O_{44}$	$Cd_{35}Se_{20}C_{330}H_{480}N_{30}O_{60}$
formula weight	9337.06	11340.64
space group	*Cmcm*	*Cmcm*
a/Å	36.837(10)	36.837(10)
b/Å	44.172(12)	44.172(12)
c/Å	35.269(10)	35.269(10)
a/°	90	90
b/°	90	90
g/°	90	90
V/Å^3	57388(27)	57388(27)
Z	4	4
temperature (K)	130(2)	130(2)
radiation (l, Å)	0.71073	0.71073
r (calcd.), g cm^{-3}	1.081	1.313
m (Mo Ka), mm^{-1}	2.423	2.580
q max, deg.	11.39	11.39
no. of data collected	38548	38568
no. of data used	2761	2762
no. of parameters	136	148
R_1 [$I > 2s(I)$]	0.1969	0.1822
wR_2 [$I > 2s(I)$]	0. 4961	0.4715
R_1 [all data]	0. 2458	0.2288
wR_2 [all data]	0.5222	0.4977
GOF	1.639	1.535
R_{int}	0.1662	0.1590

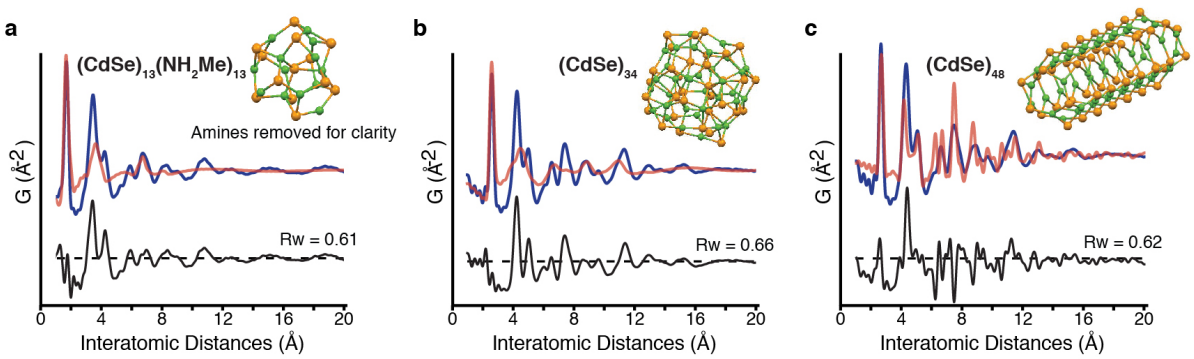

Figure S3. Optimized model PDFs of previously assigned CdSe magic-sized QDs, $(CdSe)_{13}(NH_2Me)_{13}$, $(CdSe)_{34}$, and $(CdSe)_{48}$ as calculated by Nguyen and Kasuya.[1,2] The blue line corresponds to experimental data, the red line to simulated data, and the black to the residual signal not accounted for by the simulation. The first structure is compared with the experimental PDF data of **CdSe$_{(350\ nm)}$** while $(CdSe)_{34}$ and $(CdSe)_{48}$ are compared to **CdSe$_{(380\ nm)}$**. For each example, the large residual signal not fit by the model ($\mathbf{R_w}$) demonstrates that these structures differ strongly from those isolated in this study. Prediction of "magic size" clusters can be improved in comparison to experiment by using benchmarked first principle methods, as recently reported by Nguyen et al.[3]

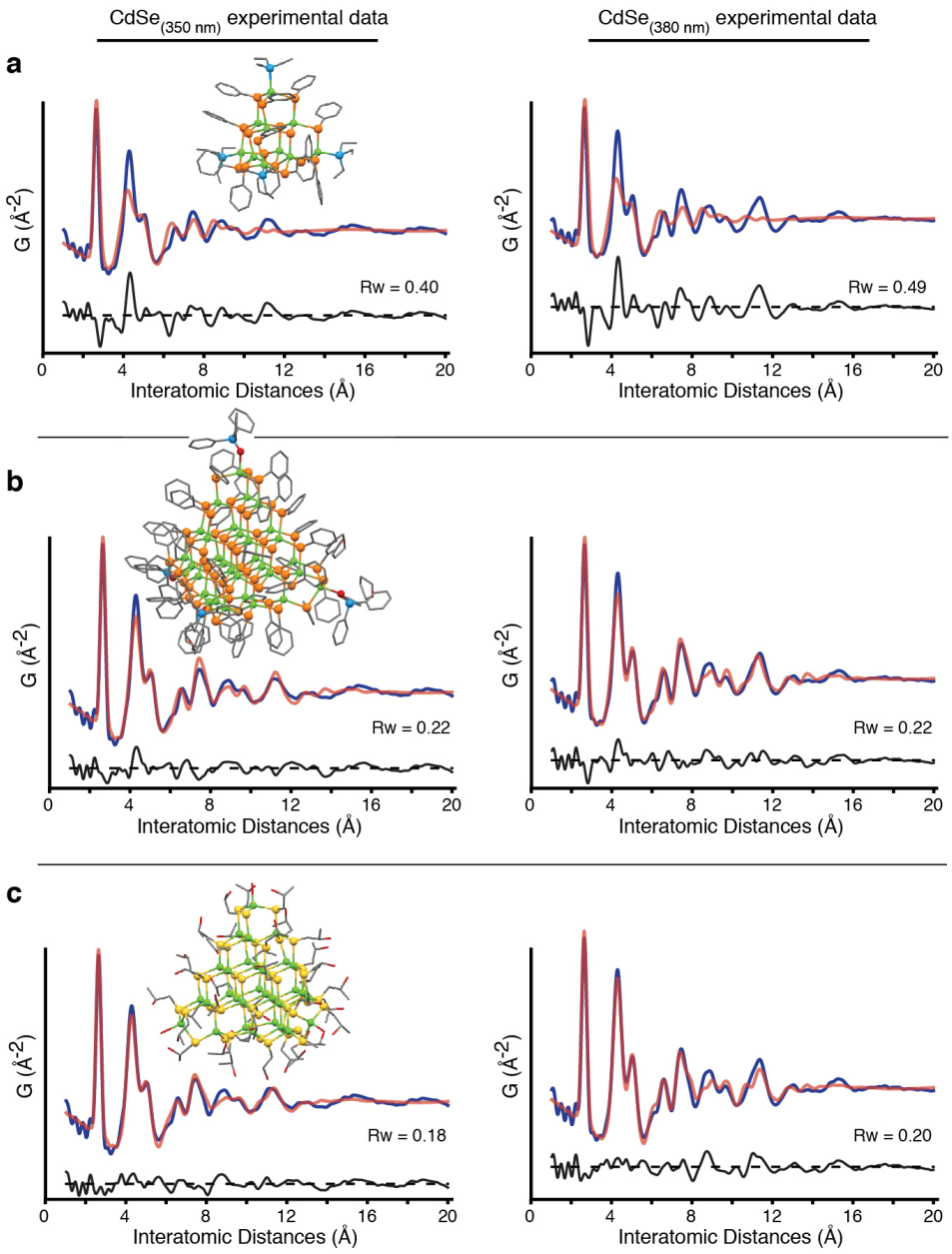

Figure S4. Optimized model PDFs of chalcogenolate clusters. The blue line corresponds to experimental data, the red line to simulated data, and the black to the residuals. Structures are colored as: Cd = green; Se = orange; S = yellow; P = blue; O = red; and C = grey. A search of the Cambridge Structural Database for high quality structures of similar size and composition to the reported QDs yielded three candidate clusters. Both a) $[Cd_{10}Se_4(SePh)_{12}(PEt3)_4]$ and b) $[Cd_{32}Se_{14}(SePh)_{36}(OPPh_3)_4]$ were reported by Eichhöfer.[4] c) $[Cd_{32}S_{14}(SCH_2CH(OH)CH_3)_{36}\bullet 4H_2O]$ was reported by Weller et al. and resembles other seminal examples of chalcogenolate clusters reported by Dance or Herron and Wang.[5–7] Before PDF simulation, the sulfur atoms in this cluster were replaced by selenium atoms, and the lattice constant was expanded to better reflect the longer cadmium selenide bond length. All three of these clusters were compared to the experimental PDFs of both **CdSe$_{(350\ nm)}$** and **CdSe$_{(408\ nm)}$**. Qualitative differences between the simulated and experimental PDFs are reflected by higher $\mathbf{R_w}$ values and stress the sensitivity and reliability of PDF fitting methods. Despite similarities in shape and composition, the PDF modeling distinguishes between chalcogenolate clusters and the reported structures.

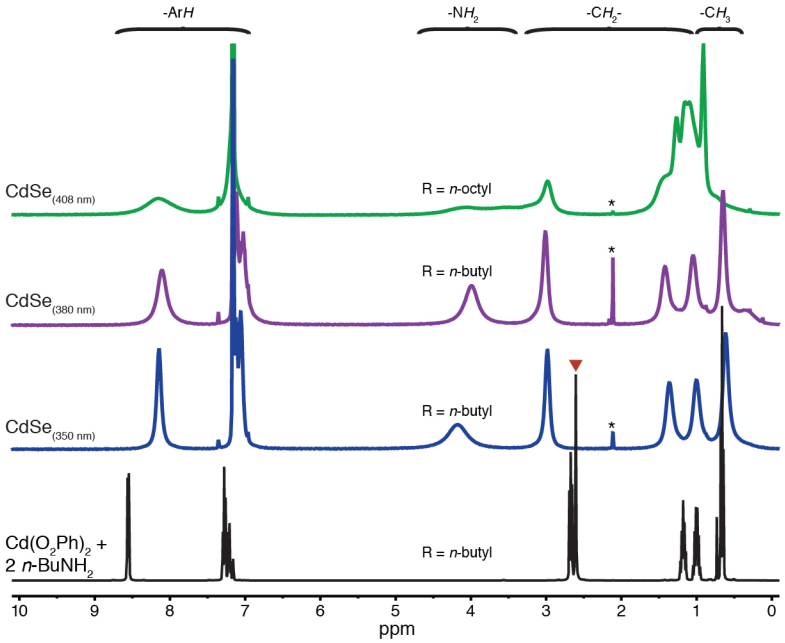

Figure S5. ^{1}H NMR spectra of $Cd(O_2CPh)_2{\cdot}(n\text{-}BuNH_2)_2$ (bottom, black), **CdSe$_{(350\ nm)}$** (bottom/middle, blue), **CdSe$_{(380\ nm)}$** (bottom/top, purple), and **CdSe$_{(408\ nm)}$** (top, green) in benzene-d_6. To acquire the spectrum of **CdSe$_{(408\ nm)}$,** a ligand exchange was performed, substituting *n*-butylamine for *n*-octylamine. A star (*) marks a residual toluene solvent impurity, and a red triangle labels the –NH_2 resonance of $Cd(O_2CPh)_2{\cdot}(n\text{-}BuNH_2)_2$, which is substantially shifted from its location in the ^{1}H NMR spectra of the QDs.

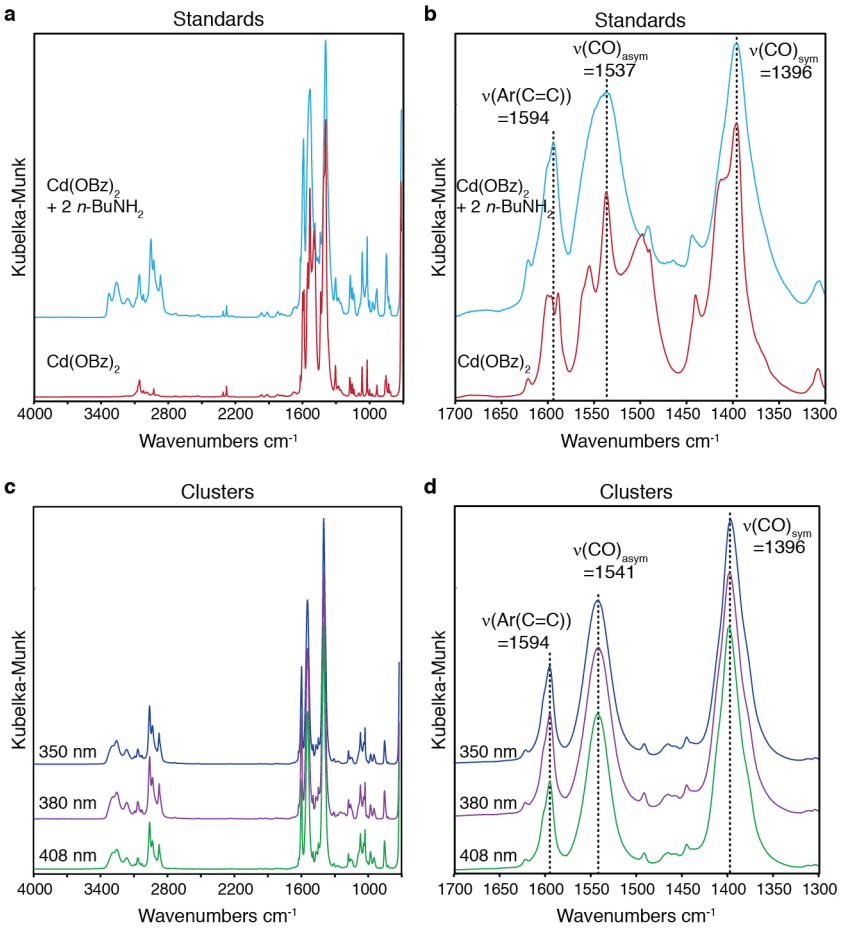

Figure S6. Diffuse Reflectance Infrared Fourier Transform Spectroscopy (DRIFTS) of $Cd(O_2CPh)_2$, $Cd(O_2CPh)_2{\cdot}(n\text{-}BuNH_2)_2$ (**a, b**), **CdSe$_{(350\ nm)}$**, **CdSe$_{(380\ nm)}$**, and **CdSe$_{(408\ nm)}$** (**c, d**). The spectra unambiguously support the presence of benzoate and amine surface ligands.

Table S2. The effect of curvature on the ligand packing density.

Cluster	QD edge length (nm)	QD surface area (nm^2)	Ligand binding sites	Ligand binding density (ligands/nm^2)	Volume of ligand shell on tetrahedron (nm^3)	Volume of ligand shell on planar surface of equivalent area (nm^3)	Factor of volume increase from curvature	Calculated density of C, H, N, O atoms in ligand shell (atoms/nm^3)	Calculated density of C, H, N, O atoms of ligands on a planar surface (atoms/nm^3)
$CdSe_{(350\ nm)}$	1.71	5.06	60	11.8	11.4	3.85	2.95	79.3	234
$CdSe_{(380\ nm)}$	2.14	7.93	84	10.6	15.0	6.03	2.48	84.3	209
$CdSe_{(408\ nm)}$	2.57	11.44	112	9.79	19.0	8.69	2.19	88.2	193

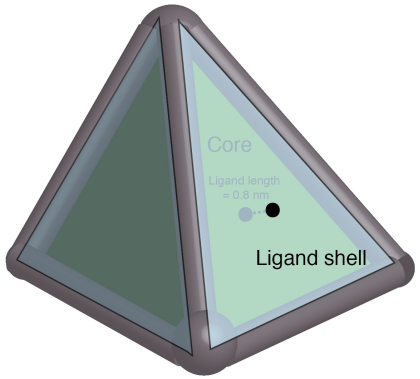

We performed a series of calculations to determine the effect of curvature on the ligand packing density. In Table 2 above, we compare ligand packing on a tetrahedral surface to ligand packing on a flat surface. The three QDs are modeled as tetrahedra with the corner cadmium atom to corner cadmium atom distance used as the edge length. The volume of the ligand layer surrounding the QD is approximated by calculating the difference between the QD core (green tetrahedron) and the volume of a larger tetrahedron with rounded edges and corners (rounded shell). The surface of this larger tetrahedron is 0.76 nm above the faces of the QD core, which is approximately the distance between cadmium and the most distal hydrogen on a datively-bound *n*-butylamine ligand. We compare the volume and density of ligands in this rounded ligand shell to ligands packed on a planar surface with the same total surface area. On the tetrahedron representing **$CdSe_{(350\ nm)}$**, the volume of the ligand shell is nearly three times greater than the volume of the ligand shell on an equivalent planar surface. As the tetrahedron increases in size, the effect of curvature on ligand shell volume diminishes though the effect is still significant: the volume of the ligand shell on the tetrahedron representing **$CdSe_{(408\ nm)}$** remains two times greater than the volume of a ligand shell on an equivalent planar surface.

Based on the rounded shell model, the atomic density of C, H, N, and O is estimated to be ~80 - 90 atoms/nm^3. This value is lower than the volume densities reported in crystal structures of representative ammonium benzoate ammonium salts (105 atoms/nm^3) (Table S3). Thus the ligand shell on our QDs is less densely packed than a typical organic crystal perhaps explaining the ligand shell disorder encountered in the single crystal diffraction studies. On a planar surface rather than a tetrahedron, the volume density is ~210 atoms/nm^3, which is greater than the volume density of diamond (176 atoms/nm^3), a purely covalent, close-packed structure that can be considered an upper limit.

Table S3. Volume density of ammonium benzoate salts reported in the Cambridge Structural Database

Compound Name	CSD Code	Density (g/cm^3)	Density ($atoms/nm^3$)
Guanidinium Benzoate	GIHCIK	1.194	95.237
Imidazolum Benzoate	HEPXUW	1.315	99.921
Ammonium Benzoate	YABFEO01	1.275	104.834
3-Phenylpropylammonium Benzoate	MOKTUC	1.214	107.955
Triethylammonium Benzoate	EPEDUZ	1.156	115.339

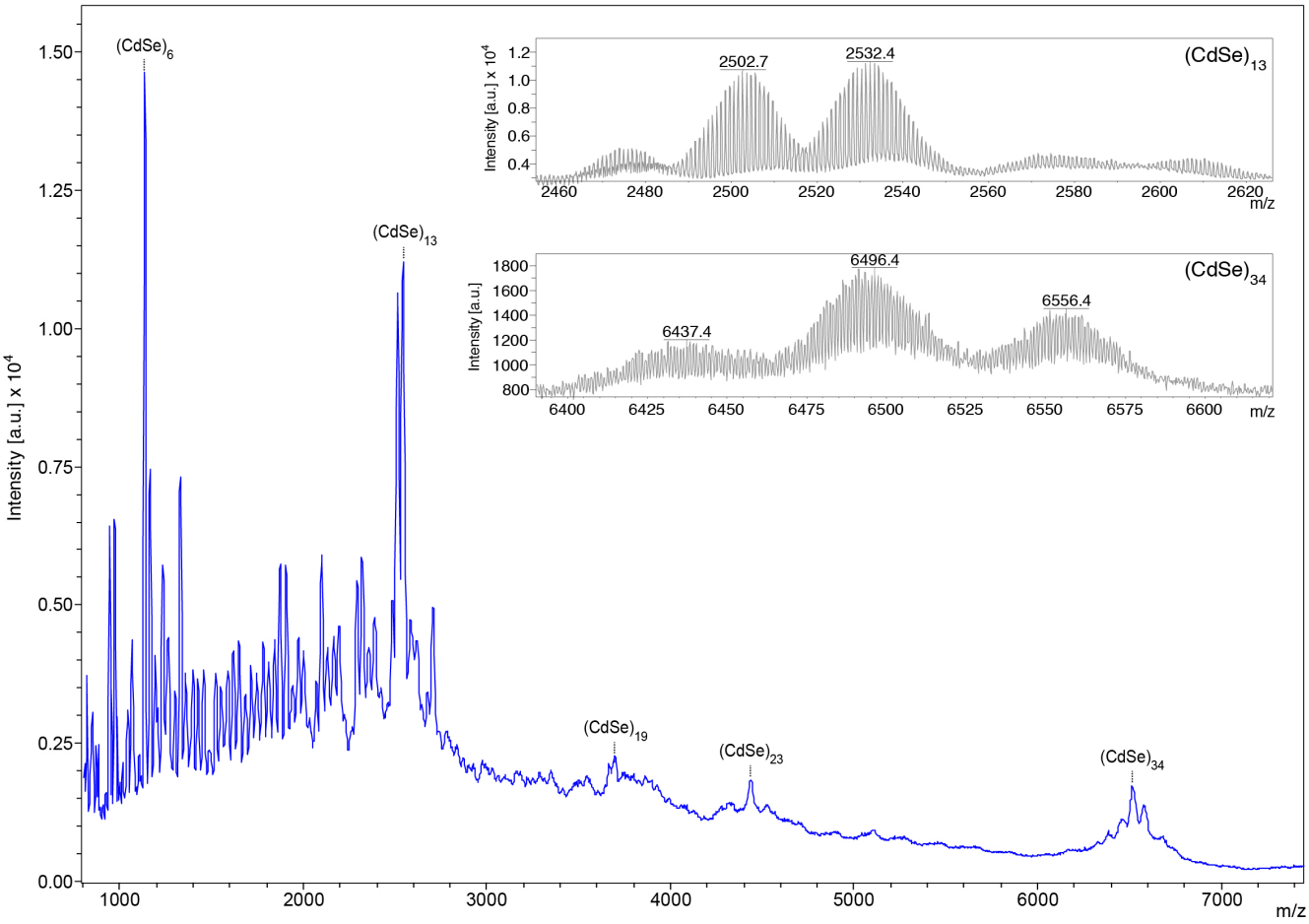

Figure S7. Laser desorption ionization mass spectrum of **CdSe$_{(350\ nm)}$** prepared by drop-casting a 0.2 mg/mL solution of **CdSe$_{(350\ nm)}$** in toluene onto a target plate. The sample was sent to Bruker and analyzed on a Bruker UltrafleXtreme operating in positive ion, reflector mode. External calibration was performed with insulin. For this sample, 30,000 shots were recorded at a laser rep rate of 1000 Hz. Laser power was set to above threshold. Ion source voltage 1 was 25 kV, ion source voltage 2 was 22.35 kV, lens voltage was 7.5 kV, and PIE delay was 190 ns.

The wide window spectrum shows a series of fragments corresponding to various stoichiometric species stable in the gas-phase. The excerpts in the upper right show fragments corresponding to $(CdSe)_{13}$ and $(CdSe)_{34}$. Simulations of these fragments do not exactly align with the observed peaks and are shifted by about 30 m/z units, which perhaps can be attributable to reaction with dioxygen. The overall fragmentation pattern, however, closely resembles fragmentation patterns previously reported for other CdSe materials with distinct absorbance profiles.[2] As such, we think that the LDI data do not reflect the true composition of our sample.

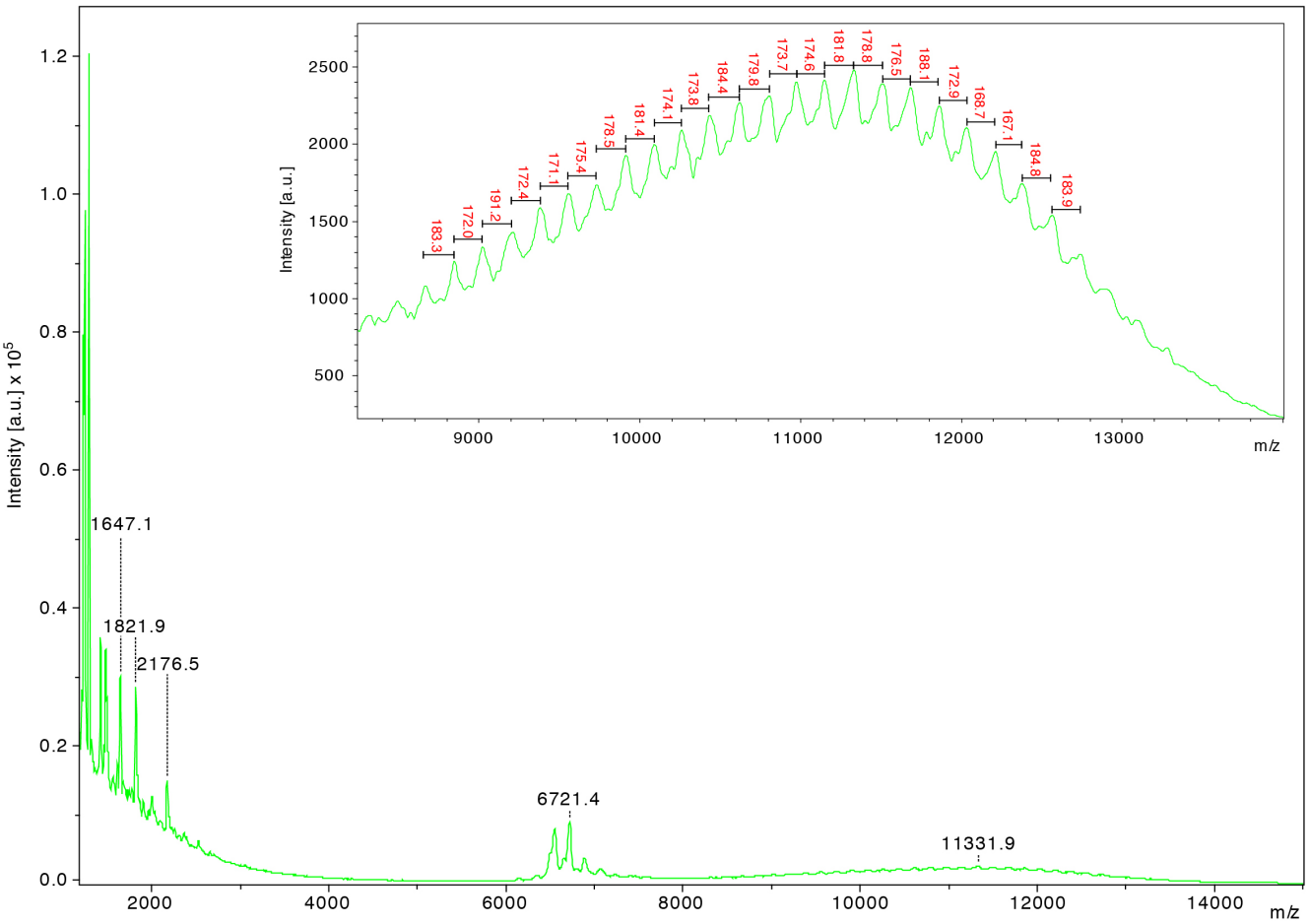

Figure S8. Matrix assisted laser desorption ionization mass spectrum of **CdSe$_{(350\ nm)}$** prepared by drop-casting a 20.0 mg/mL solution of **CdSe$_{(350\ nm)}$** in toluene with 2-[(2E)-3-(4-*tert*-butylphenyl)-2-methylprop-2-enylidene]malononitrile (DCTB) as a matrix onto a target plate. The sample was sent to Bruker and analyzed on a Bruker UltrafleXtreme operating in positive ion, linear mode. External calibration was performed with insulin.

The wide window spectrum shows a series of cadmium selenide fragments, including a species in the range of $(CdSe)_{34}$ and demonstrates the absence of a distinct parent ion peak for **CdSe$_{(350\ nm)}$** at 11,346 m/z. Instead, as shown in the excerpt in the upper right, this region exhibits a broad, low intensity feature with distinct peaks differing in mass by approximately one cadmium selenide unit.

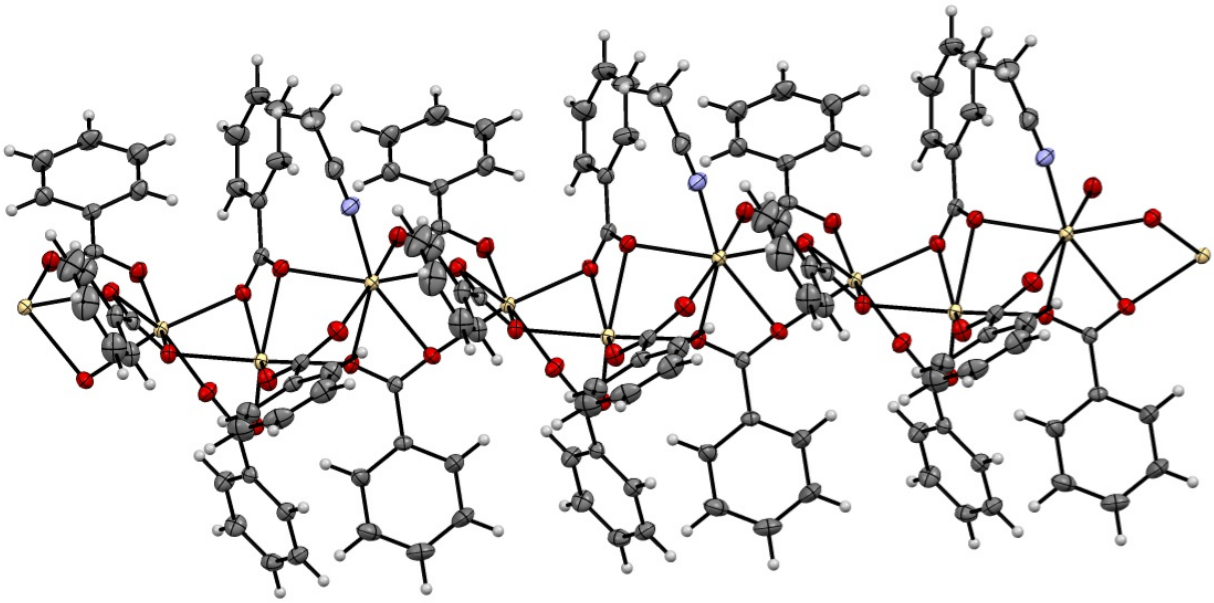

Figure S9. A view of $[(Cd(O_2CPh)_2)_3(CH_3CN)]_n$ showing three repeat units. Thermal ellipsoids are set at the 50% probability level. Grey ellipsoids = carbon; red ellipsoids = oxygen; yellow ellipsoids = cadmium; blue ellipsoids = nitrogen; white spheres = hydrogen.

Table S4. $[(Cd(O_2CPh)_2)_3(CH_3CN)]_n$ single crystal, intensity collection and refinement data.

	$[(Cd(O_2CPh)_2)_3(CH_3CN)]_n$
lattice	Monoclinic
formula	$C_{44}H_{33}Cd_3NO_{12}$
formula weight	1104.91
space group	$P2_1/c$
a/Å	17.0374(12)
b/Å	9.1839(6)
c/Å	26.2103(18)
α/°	90
β/°	95.0770(10)
γ/°	90
V/Å^3	4085.0(5)
Z	4
temperature (K)	150(2)
radiation (λ, Å)	0.71073
ρ (calcd.), g cm^{-3}	1.797
μ (Mo Ka), mm^{-1}	1.613
θ max, deg.	30.66
no. of data collected	64743
no. of data used	12607
no. of parameters	542
R_1 [$I > 2\sigma(I)$]	0.0292
wR_2 [$I > 2\sigma(I)$]	0.0562
R_1 [all data]	0.0421
wR_2 [all data]	0.0606
GOF	1.048
R_{int}	0.0397

REFERENCES

(1) Nguyen, K. A.; Day, P. N.; Pachter, R. *J. Phys. Chem. C* **2010**, *114*, 16197.
(2) Kasuya, A.; Sivamohan, R.; Barnakov, Y. A.; Dmitruk, I. M.; Nirasawa, T.; Romanyuk, V. R.; Kumar, V.; Mamykin, S. V.; Tohji, K.; Jeyadevan, B.; Shinoda, K.; Kudo, T.; Terasaki, O.; Liu, Z.; Belosludov, R. V.; Sundararajan, V.; Kawazoe, Y. *Nat. Mater.* **2004**, *3*, 99.
(3) Nguyen, K. A.; Pachter, R.; Day, P. N. *J. Chem. Theory Comput.* **2013**, *9*, 3581.
(4) Eichhöfer, A. *Eur. J. Inorg. Chem.* **2005**, *2005*, 1245.
(5) Vossmeyer, T.; Reck, G.; Schulz, B.; Katsikas, L.; Weller, H. *J. Am. Chem. Soc.* **1995**, *117*, 12881.
(6) Dance, I. G.; Choy, A.; Scudder, M. L. *J. Am. Chem. Soc.* **1984**, *106*, 6285.
(7) Herron, N.; Calabrese, J. C.; Farneth, W. E.; Wang, Y. *Science* **1993**, *259*, 1426.